第 30 卷第 4 期 无 机 化 学 学 报 Vol.30 No.4
2014 年 4 月 CHINESE JOURNAL OF INORGANIC CHEMISTRY 733-740

# 介孔碳纳米纤维–硫作为锂硫电池正极材料

赵 斌[1] 李念武*,[2] 吕洪岭[2] 林子夏[1] 郑明波*,[1]
([1]南京大学,微结构国家实验室,电子科学与工程学院,南京 210093)
([2]南京航空航天大学,材料科学与技术学院,纳米材料研究所,南京 210016)

**摘要**:锂硫电池的商用化受到硫和多硫化锂低的电导率、多硫化锂在有机电解液中的溶解、放电过程中硫的体积膨胀等因素的制约。我们通过自模板法制备了具有石墨化孔壁结构的介孔碳纳米纤维(MCNF),并利用这种结构将硫和多硫化锂封装在碳骨架内。具有石墨化孔壁结构的一维 MCNF 能够在循环中为硫和多硫化锂提供良好的导电网络。MCNF 中小的介孔能够抑制长链多硫化锂的扩散。另外,MCNF 大的孔容能够负载比较多的硫,并且能够为硫的放电膨胀提供足够的纳米空间。本工作制备的 MCNF-硫纳米复合材料在 0.8 $A\cdot g^{-1}$ 的电流密度下,经过 100 次循环后仍有 820 $mAh\cdot g^{-1}$ 的比容量。

**关键词**:纳米结构;介孔材料;电化学;能量转换;锂硫电池
**中图分类号**:O613.51;O614.111 **文献标识码**:A **文章编号**:1001-4861(2014)04-0733-08
**DOI**:10.11862/CJIC.2014.151

## Mesoporous Carbon Nanofiber-Sulfur Cathode for Lithium-Sulfur Batteries

ZHAO Bin[1] LI Nian-Wu*,[2] LU Hong-Ling[2] LIN Zi-Xia[1] ZHENG Ming-Bo*,[1]
([1]*Nanjing National Laboratory of Microstructures, School of Electronic Science and Engineering, Nanjing University, Nanjing* 210093, *China*)
([2]*Nanomaterials Research Institute, College of Materials Science and Technology, Nanjing University of Aeronautics and Astronautics, Nanjing* 210016, *China*)

**Abstract:** Rechargeable lithium-sulfur batteries′ commercial applications are still hindered by some major basic obstacles, such as the low electrical conductivity of sulfur and polysulfides, the dissolution of lithium polysulfides in organic electrolyte, and the volume expansion of sulfur during discharge. In this study, a mesoporous carbon nanofiber (MCNF) with graphitic pore wall prepared by an easy self-template strategy was designed to encapsulate sulfur and polysulfides in the carbon framework. The one-dimensional MCNF with graphitic pore wall can provide an effective conductive network for sulfur and polysulfides during cycling. The small mesopore of MCNF can also restrain the diffusion of long-chain polysulfides. Furthermore, MNCF with high volume can encapsulate a relatively high amount of sulfur and provide internal void space to accommodate volume expansion during discharge. The resulting MCNF-sulfur nanocomposite shows high and stable specific capacities of 820 $mAh\cdot g^{-1}$ after 100 cycles at a rate of 0.8 $A\cdot g^{-1}$.

**Key words:** nanostructures; mesoporous materials; electrochemistry; energy conversion; lithium-sulfur battery

Rechargeable lithium-sulfur batteries have promising applications in advanced energy-storage devices because of their high theoretical specific capacity (1 675 $mAh\cdot g^{-1}$) and energy density (2 600

收稿日期:2013-11-24。收修改稿日期:2014-01-12。
国家自然科学基金(No.51202106)资助项目。
*通讯联系人。E-mail:nianwuli@gmail.com,zhengmingbo@nju.edu.cn

Wh·kg$^{-1}$)[1-6]. Sulfur also possesses other advantages, such as natural abundance, low cost, and environmental benignity[1]. Nevertheless, commercial applications that use lithium-sulfur batteries have not been very successful because of the low electrical conductivity of sulfur and polysulfides, dissolution of polysulfides in organic electrolyte, and volume expansion of sulfur during discharge[5]. The dissolution of polysulfides can result in troublesome shuttling loss during cycling. During charging, the long-chain polysulfides generated at the positive electrode diffuse to the Li anode where they directly react with Li in a parasitic reaction to regenerate lower-order chain polysulfides[1,7-8]. These species diffuse back to the sulfur cathode and regenerate long-chain polysulfides. This parasitic process repeatedly occurs, creating an internal shuttling mechanism during charging. The process decreases active mass utilization and markedly reduces coulombic efficiency, thereby resulting in rapidly decreased capacity[1]. Various strategies have been developed to address these issues, including the fabrication of polymer-sulfur composites[9-11], preparation of porous carbon-sulfur composites[12-18], use of coating layers[19-22] or additives[23-24], and optimization of organic electrolyte[25-26]. Porous carbon materials are proven to be effective in confining the diffusion of polysulfides and improving the conductivity of sulfur because of their excellent conductivity, large surface area, high volume, and strong adsorption property[27-32]. The characteristics of porous carbon such as dimension, morphology, pore structure, and pore size are critical to the electrochemical performance of porous carbon-sulfur composite electrodes[14,30-31]. Notably, one-dimensional (1D) porous carbon structures offer unique features for addressing the issues of sulfur cathodes[5,33-35]. The 1D carbon nanofiber provides better electrical connection to sulfur[5], thus the 1D carbon nanofiber-sulfur nanocomposite can deliver a high initial discharge capacity of approximately 1 400 mAh·g$^{-1}$ [34-35]. Cui et al.[33] demonstrated that a 1D hollow carbon nanofiber with high aspect ratio can reduce the random diffusion of polysulfides in an organic electrolyte, whereas the thin carbon wall allows fast transport of lithium ions. Aurbach et al.[36] showed that carbon nanofibers with micropores can effectively restrain polysulfide diffusion. Therefore, the design of 1D carbon nanofibers with suitable pore structure can potentially help to solve the above mentioned difficulties in engineering sulfur cathodes.

Herein, a mesoporous carbon nanofiber (MCNF) with bimodal pore structure, graphitic pore wall, and high pore volume was prepared by an easy self-template method (Fig.1). The graphitic pore wall of MCNF can effectively provide a conductive network for sulfur and polysulfides. The MCNF with high pore volume can encapsulate a relatively high amount of sulfur and provide an internal void space to accommodate volume expansion during discharge. The small mesopores of MCNF can also restrain the diffusion of long-chain polysulfides. Therefore, the as-prepared MCNF-S nanocomposite shows good lithium-sulfur battery performance.

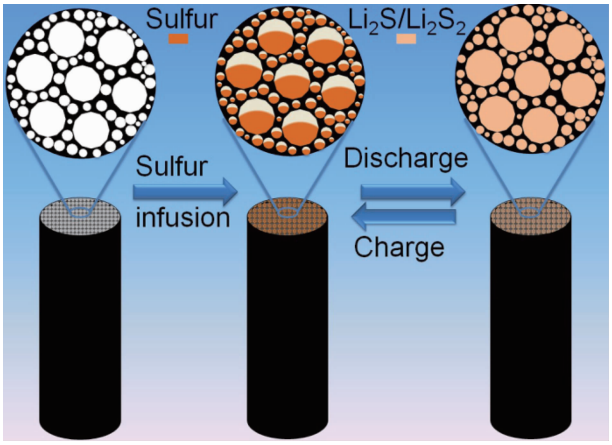


Fig.1 Schematic of MCNF-S nanocomposite during discharge-charge

## 1 Experimental

### 1.1 Sample preparation

In a typical procedure, zinc acetate (8.0 g) was added to ethylene glycol (150 mL), the mixture was stirred at 70 ℃ for 1 h, and then followed by a hydrothermal treatment at 150 ℃ for 5 h under static conditions. The solution was dumped and the slurry was collected, followed by calcination at 600 ℃ for 2 h in $N_2$ (Heating rates were 5 ℃·min$^{-1}$ below 400 ℃ and 2 ℃·min$^{-1}$ above 400 ℃). The composite was

immersed in a 10% HCl solution (200 mL) with stirring overnight. The sample was washed with water several times and then heated at 900 ℃ for 5 h, with a heating rate of 5 ℃·min$^{-1}$, under $N_2$. The MCNF was thus obtained.

A 200 mg portion of MCNF was mixed with 400 mg of the sublimed sulfur and was pulverized for 30 min in an agate mortar. Afterwards, the mixture was heated to 155 ℃ and maintained at this temperature for 24 h in a Teflon-lined autoclave, yielding the MCNF-S nanocomposite.

Mesoporous carbon CMK-3 was prepared by using SBA-15 silica as the hard template[19]. The preparation procedure of CMK-3-S nanocomposite was the same as that for MCNF-S.

### 1.2 Material characterization

X-ray diffraction (XRD) patterns ($2\theta$ angle from 20° to 80°) were collected on a D8-ADVANCE powder X-ray diffractometer operating at 5°·min$^{-1}$ (40 kV, 40 mA, Cu $K\alpha$ radiation, $\lambda$=0.154 18 nm, Ni filter, scintillation counter, LynxEye array detector). The microstructure of the samples was examined with a Hitachi S-4800 field-emission scanning electron microscope (FE-SEM) operating at a voltage of 10 kV and a JEOL JEM-2100 transmission electron microscope (TEM) at an accelerating voltage of 200 kV. $N_2$ adsorption-desorption analysis was performed using a Micromeritics ASAP 2010 instrument at 77 K. Thermal analysis was performed on NETZSCH STA 409C thermal analyzer, in which the sample was heated in alumina crucible under $N_2$ flow to 600 ℃ at a heating rate of 10 ℃·min$^{-1}$.

### 1.3 Electrochemical test

The cathode slurry was prepared by mixing 70wt% MCNF-S nanocomposite, 20wt% Super P (TIMCAL, Graphite & Carbon Inc.), and 10wt% of polyvinylidene difluoride (PVDF, Alfa Aesar) dissolved in *N*-methyl-2-pyrrolidone (NMP, Sigma-Aldrich). Positive electrodes were produced by coating the slurry on aluminum foil and drying at 60 ℃ for 12 h. Each current collector contains between 0.9 mg·cm$^{-2}$ to 1.0 mg·cm$^{-2}$ active material. Cell tests were carried out using 2032 coin-type cells cycled at room temperature between 1.0 V and 3.0 V, which were fabricated in an argon-filled glove box using lithium metal as the reference and counter electrodes, and Celgard 2250 film as the separator. The electrolyte was 1 mol·L$^{-1}$ bis-(trifluoromethane)sulfonamide lithium (LiTFSI) in a mixed solvent of dimethoxyethane (DME) and dioxolane (DOL) with a volume ratio of 1:1. Cells performance was tested with LAND CT-2100A instrument (Wuhan, China). The specific capacity was calculated based on the mass of elemental sulfur. Cyclic voltammetry measurement was performed using a CHI 660D electrochemical workstation (Shanghai Chenhua, China) at a scan rate of 0.1 mV·s$^{-1}$.

## 2 Results and discussion

ZnO/carbon composites with fibrous structure, shown in Figs.2a and 2b, were obtained by carbonizing at 600 ℃ using zinc glycolate as the template. The ZnO nanofibers, given in Fig.2c, resulted from heating the ZnO/carbon composites in the air at 600 ℃. During the heat treatment process, the organic units are carbonized into carbon frameworks, whereas the zinc ions are *in-situ* crystallized into zinc oxides[37] as evidenced by XRD patterns (Fig.2d). All diffraction peaks are well consistent with the wurtzite-type ZnO (PDF card 36-1451). MCNF is obtained after removing the ZnO template and carbonizing at 900 ℃. After heating the sulfur and MCNF mixture at 155 ℃ for 24 h, the sublimed sulfur was infused into the mesopores of MCNF, and the MCNF-S nanocomposite was obtained.

Fig.3 shows SEM and TEM images of MCNF and MCNF-S nanocomposite. MCNF retains the fibrous morphology with diameters of 300 nm to 500 nm and a length of 50 μm (Figs.3a and 3b). The MCNF surface shows numerous protuberances (Fig.3c), and multiple MCNFs are bundled together. MCNF has many interconnected mesopores (Fig.3c) that are conductive to melted sulfur diffusion. Notably, the pore wall of MCNF has a graphitic structure (Fig.3c inset), which is advantageous for improving the conductivity of sulfur particles. After the sulfur-infusion process, the nanofiber structure is retained

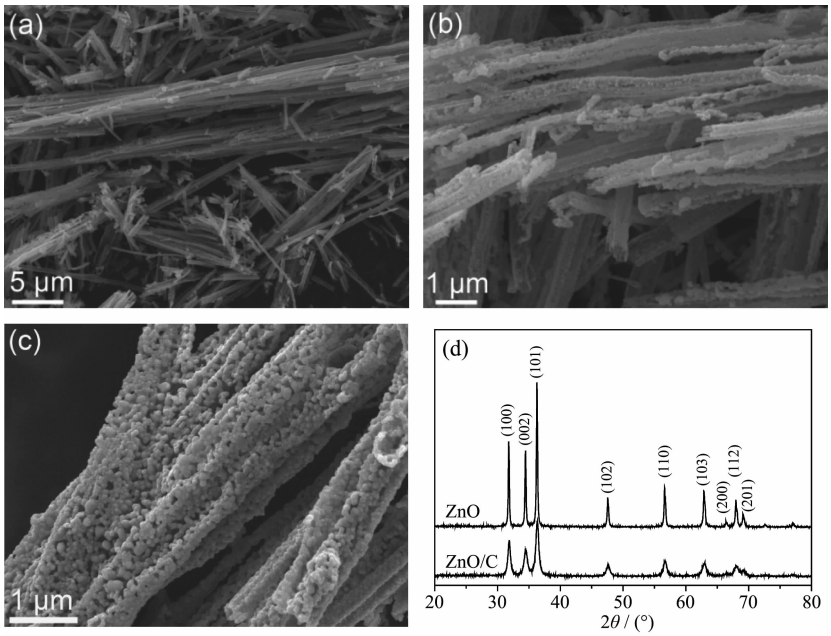


Fig.2 (a, b) SEM images of ZnO/carbon composites, (c) SEM image of ZnO nanofibers, (d) XRD patterns of the ZnO/carbon composite (ZnO/C) and ZnO nanofibers

(Figs.3d and 3e), and the mesoporous structure is filled with sulfur particles (Fig.3f). Elemental mapping reveals that carbon and sulfur are narrowly distributed in the MCNF-S nanocomposite (Fig.3g to 3i).

The isotherm for $N_2$ adsorption-desorption of the MCNF nanocomposite exhibits a hysteresis between the adsorption and desorption branches at $P/P_0$=0.3~0.8 (Fig.4a), indicating the mesoporous structure of MCNF. MCNF has a BET specific surface area of 1 008 $m^2 \cdot g^{-1}$ and a high pore volume of 1.98 $cm^3 \cdot g^{-1}$. The pore size distribution curve of MCNF (Fig.4b) shows two peaks at 2.50 nm and 6.38 nm. Compared with MCNF, the MCNF-S nanocomposite has a lower BET surface area of 92 $m^2 \cdot g^{-1}$ and a lower pore volume of 0.3 $cm^3 \cdot g^{-1}$. Furthermore, MCNF-S nanocomposite exhibits a hysteresis at $P/P_0$=0.4~0.8 (Fig.4a), indicating that MCNF-S nanocomposite also has a mesoporous structure. The pore size distribution curve of MCNF-S nanocomposite (Fig.4b) presents one small peak at about 10 nm, indicating that the mesoporous structure of MCNF is mostly filled with sulfur. The XRD patterns of sulfur, MCNF, and MCNF-S nanocomposite are shown in Fig.4c. Sulfur exists in a crystalline state with an orthorhombic structure. For the MCNF-S nanocomposite, the sharp diffraction peaks of sulfur disappear, further demonstrating that sulfur exists as tiny particles and in a highly dispersed state with low-molecular-weight monolayered coverage inside the MCNF-S nanocomposite[8,19,36]. The thermal analysis result (Fig.4d) shows that the sulfur content is 66.2% for the MCNF-S nanocomposite.

Fig.5a shows cyclic voltammetry measurement of the MCNF-S nanocomposite. The two evident reduction peaks are located at 2.2 V and 2.0 V. These two peaks can be attributed to the reduction of the $S_8$ ring to long-chain lithium polysulfides and the reduction of long-chain lithium polysulfides to $Li_2S_2$ and $Li_2S$[21,25,35], respectively, and correspond to the two discharge plateaus in the discharge curve (Fig.5b). An anodic peak at 2.48 V (Fig.5a) can be attributed to the oxidation of $Li_2S$ and $Li_2S_2$[35]. Fig.5c shows that the as-prepared MCNF-S nanocomposite has an initial specific discharge capacity of 1 457 $mAh \cdot g^{-1}$ at 0.2 $A \cdot g^{-1}$. After the initial discharge, the MCNF-S nanocomposite delivers a discharge capacity of 1 270 $mAh \cdot g^{-1}$ at the second cycle and maintains at 841 $mAh \cdot g^{-1}$ after 50 cycles at 0.2 $A \cdot g^{-1}$ (Fig.5b). Furthermore, the coulombic efficiency is within the range of 97% to 99% after the first few cycles (Fig.5c).

The MCNF-S nanocomposite acquires a capacity

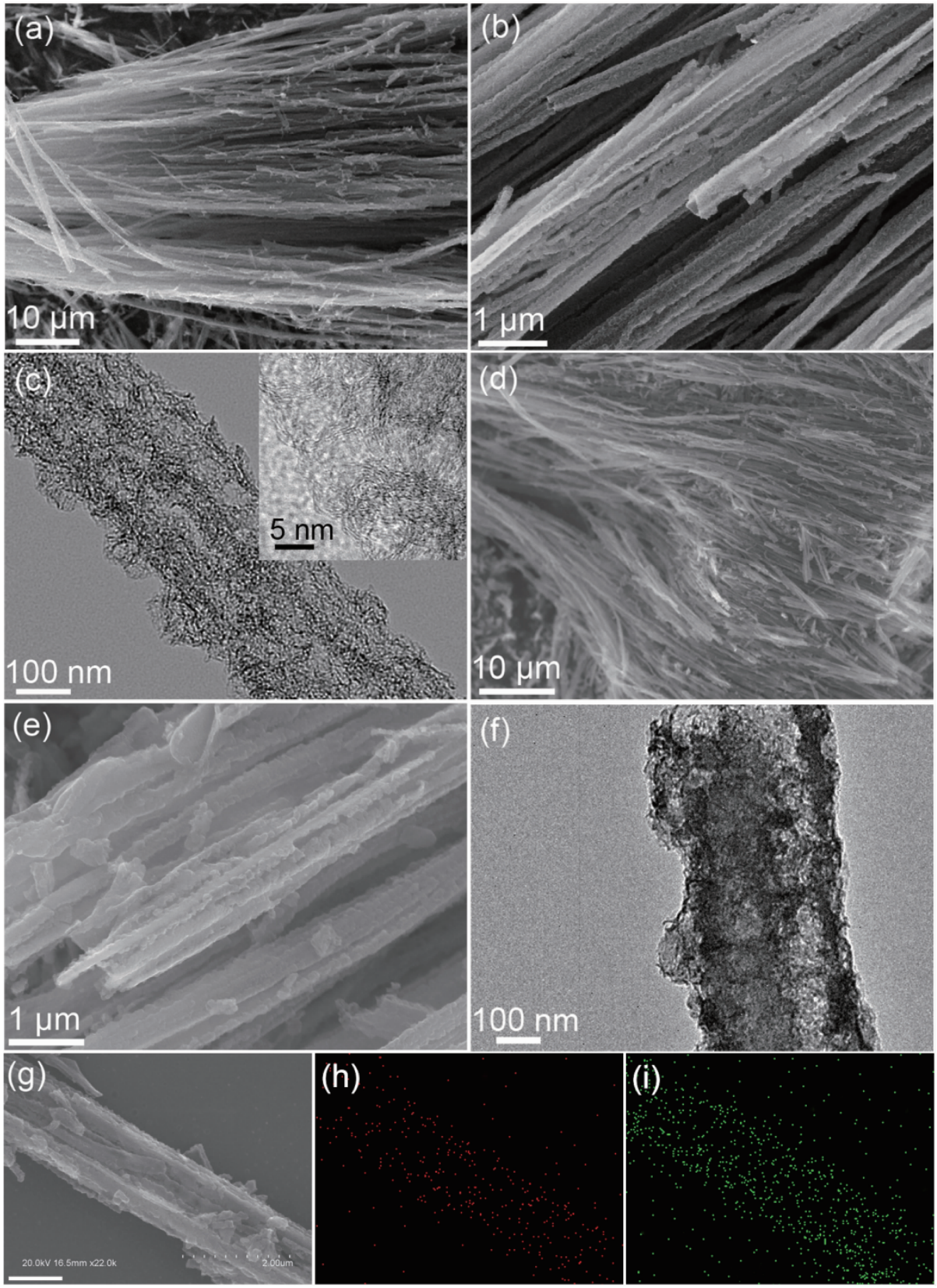


Fig.3　(a, b) SEM images of MCNF; (c) TEM images of MCNF; the inset is HRTEM image of MCNF, (d, e) SEM images of MCNF-S nanocomposite, (f) TEM image of MCNF-S nanocomposite, SEM image of MCNF-S nanocomposite (g) and the corresponding elemental mapping of carbon (h) and sulfur (j), the scale bar in (g) is 1 μm

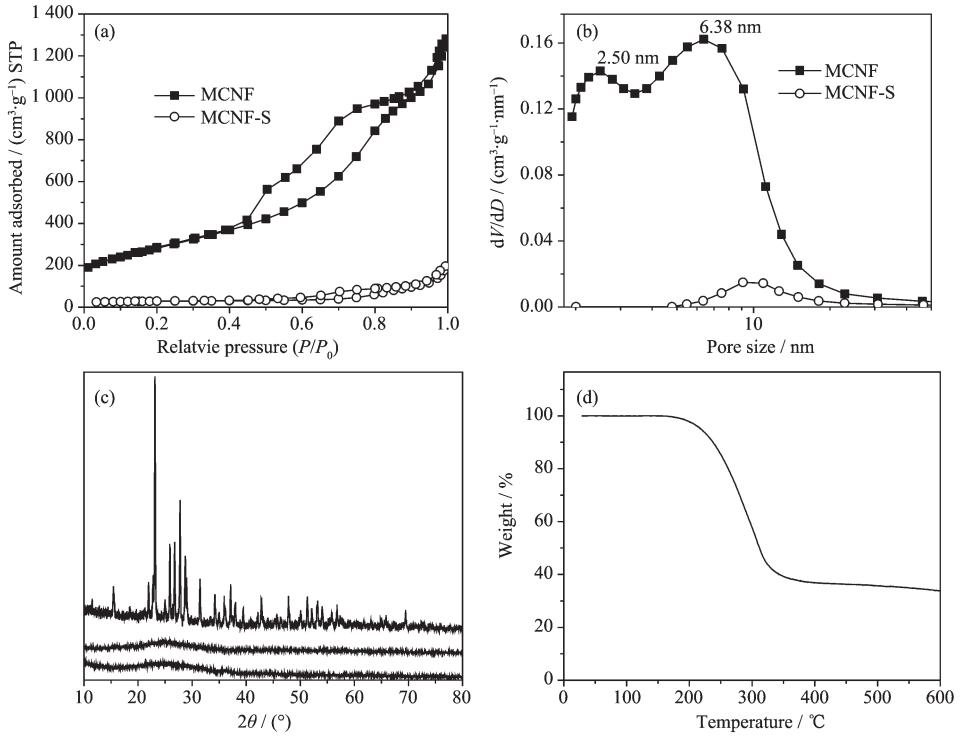


Fig.4 $N_2$ sorption isotherms (a) and pore size distribution curves (b) of the MCNF and MCNF-S nanocomposite, (c) XRD patterns of S, MCNF, and MCNF-S nanocomposite, (d) Thermal analysis curve of MCNF-S nanocomposite

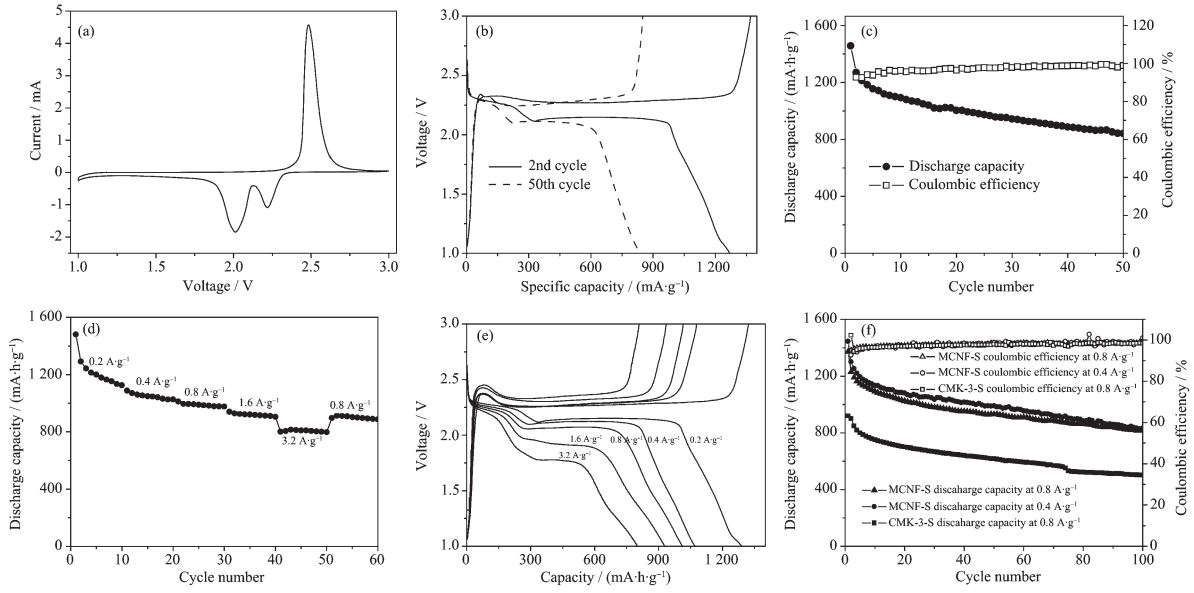


Fig.5 (a) Cyclic voltammogram of MCNF-S nanocomposite at 0.1 mV·s$^{-1}$ scanning rate, (b) Discharge-charge voltage profiles of MCNF-S nanocomposite at 0.2 A·g$^{-1}$, (c) Cycle life and coulombic efficiency of the MCNF-S nanocomposite at 0.2 A·g$^{-1}$, (d) Rate capability of the MCNF-S nanocomposite, (e) Typical voltage capacity profiles of the MCNF-S nanocomposite at various rates, (f) Cycle life and coulombic efficiency of the MCNF-S nanocomposite at rates of 0.4 A·g$^{-1}$ and 0.8 A·g$^{-1}$ and the CMK-3-S nanocomposite at a rate of 0.8 A·g$^{-1}$

of 801 mAh·g$^{-1}$ at a current rate of 3.2 A·g$^{-1}$ (Fig.5d). When the current rate is increased from 0.2 A·g$^{-1}$ to 3.2 A·g$^{-1}$, the MCNF-S nanocomposite maintains the typical two-plateau behavior of the sulfur cathode (Fig. 5e). Furthermore, most of the discharge capacity is recovered with increase in current density again from 3.2 A·g$^{-1}$ to 0.8 A·g$^{-1}$ (Fig.5d). This result shows the significant abuse tolerance of the MCNF-S nanocom-

posite at different current densities. To evaluate the cyclability, the sample is tested at 0.4 $A \cdot g^{-1}$ and 0.8 $A \cdot g^{-1}$ for 100 cycles (Fig.5e). The MCNF-S nanocomposite exhibits initial discharge capacities of 1 445 $mAh \cdot g^{-1}$ and 1 380 $mAh \cdot g^{-1}$ at 0.4 $A \cdot g^{-1}$ and 0.8 $A \cdot g^{-1}$, respectively (Fig.5f). After 100 cycles, the cathode retains capacities of 833 $mAh \cdot g^{-1}$ and 820 $mAh \cdot g^{-1}$ at 0.4 $A \cdot g^{-1}$ and 0.8 $A \cdot g^{-1}$, respectively. Furthermore, the coulombic efficiency is within 97% to 99% at both rates. By contrast, CMK-3-S shows much lower capacity.

The good electrochemical behavior of the as-prepared MCNF-S nanocomposite can be attributed to multiple synergistic factors that originate from its design. First, the mesopore of the MCNF has graphitic pore walls that can provide an excellent conductive network for sulfur and polysulfides. Furthermore, the 1D carbon nanofiber structure enables the rapid transport of ions and electrons[33,35]. These structure attributes of 1D MCNF are crucial in ensuring high specific capacity and good rate performance of the MCNF-S nanocomposite. Second, the high pore volume of MCNF can provide adequate internal void space to accommodate volume changes during the discharge and charge processes. The actual loading of sulfur in the MCNF-S nanocomposite is 66.2%, which is less than the theoretical maximum loading of sulfur (69.6%). Therefore, the pore structure of MCNF can provide sufficient internal void space for sulfur expansion. Third, 1D MCNF has a bimodal mesoporous structure. The small mesopores are interconnected with the larger mesopores, which facilitates the transfer of lithium ions and restrains the long-chain polysulfide diffusion[27,30-31]. Therefore, MCNF can serve as an excellent nanoelectrochemical reaction chamber for sulfur cathodes.

## 3 Conclusions

In summary, MCNF-S nanocomposite for lithium-sulfur batteries has been designed in this study. An easy self-template strategy for the synthesis of MNCF with graphitic pore wall based on hydrothermal treatment pathway has been demonstrated. The 1D carbon nanofiber structure and graphitic pore wall of the MCNF enables the rapid transport of ions and electrons, thereby ensuring the high specific capacity of the MCNF-S nanocomposite. The small mesopore structure of MCNF can restrain the diffusion of long-chain polysulfides. Lastly, the high volume of MCNF can provide adequate internal void space for sulfur expansion. Therefore, the MCNF-S nanocomposite retains a discharge capacity of 820 $mAh \cdot g^{-1}$ after 100 cycles at a rate of 0.8 $A \cdot g^{-1}$. Furthermore, the coulombic efficiency can be maintained from 97% to 99% at the same rate.

## References:


[1] Ji X L, Nazar L F. *J. Mater. Chem.*, **2010**,**20**:9821-9826

[2] Bruce P G, Freunberger S A, Tarascon J M, et al. *Nat. Mater.*, **2012**,**11**:19-29

[3] Evers S, Nazar L F. *Accounts Chem. Res.*, **2013**,**46**:1135-1143

[4] Manthiram A, Fu Y Z, Su Y S. *Accounts Chem. Res.*, **2013**, **46**:1125-1134

[5] Yang Y, Zheng G Y, Cui Y. *Chem. Soc. Rev.*, **2013**,**42**:3018-3032

[6] Tao X Y, Chen F, Xia Y, et al. *Chem. Commun.*, **2013**,**49**: 4513-4515

[7] Mikhaylik Y V, Akridge J R. *J. Electrochem. Soc.*, **2004**, **151**:A1969-A1976

[8] Li N W, Zheng M B, Lu H L, et al. *Chem. Commun.*, **2012**, **48**:4106-4108

[9] Wu F, Chen J Z, Chen R J, et al. *J. Phys. Chem. C*, **2011**, **115**:6057-6063

[10]Fu Y Z, Manthiram A. *RSC Adv.*, **2012**,**2**:5927-5929

[11]Xiao L F, Cao Y L, Xiao J, et al. *Adv. Mater.*, **2012**,**24**: 1176-1181

[12]ZHENG Jia-Fei(郑加飞), ZHENG Ming-Bo(郑明波), LI Nian-Wu(李念武), et al. *Chinese J. Inorg. Chem.*(无机化学学报), **2013**,**29**(7):1355-1360

[13]MAO Yan(毛艳), ZHANG Chuan-Hui(张传辉), ZHANG Yang(张洋), et al. *Chinese J. Inorg. Chem.*(无机化学学报), **2013**,**29**(5):889-895

[14]Zhang C F, Wu H B, Yuan C Z, et al. *Angew. Chem. Int. Edit.*, **2012**,**51**:9592-9595

[15]Cao Y L, Li X L, Aksay I A, et al. *Phys. Chem. Chem. Phys.*, **2011**,**13**:7660-7665

[16]Zhang F F, Zhang X B, Dong Y H, et al. *J. Mater. Chem.*, **2012**,**22**:11452-11454

[17]Wang H L, Yang Y, Liang Y Y, et al. *Nano Lett.*, **2011**,**11**: 2644-2647

[18]Jin J, Wen Z Y, Ma G Q, et al. *RSC Adv.*, **2013**,**3**:2558-2560

[19]Ji X L, Lee K T, Nazar L F. *Nat. Mater.*, **2009**,**8**:500-506

[20]Yang Y, Yu G H, et al. *ACS Nano*, **2011**,**5**:9187-9193

[21]Li G C, Li G R, Ye S H, et al. *Adv. Energy Mater.*, **2012**,**2**: 1238-1245

[22]Lee K T, Black R, Yim T, et al. *Adv. Energy Mater.*, **2012**, **2**:1490-1496

[23]Ji X L, Evers S, Black R, et al. *Nat. Commun.*, **2011**,**2**:325

[24]Evers S, Yim T, Nazar L F. *J. Phys. Chem. C*, **2012**,**116**: 19653-19658

[25]Shin E S, Kim K, Oh S H, et al. *Chem. Commun.*, **2013**,**49**: 2004-2006

[26]Suo L M, Hu Y S, Li H, et al. *Nat. Commun.*, **2013**,**4**:1481

[27]Liang C D, Dudney N J, Howe J Y. *Chem. Mater.*, **2009**,**21**: 4724-4730

[28]Xin S, Gu L, Zhao N H, et al. *J. Am. Chem. Soc.*, **2012**,**134**: 18510-18513

[29]Kim J, Lee D J, Jung H G, et al. *Adv. Funct. Mater.*, **2013**, **23**:1076-1080

[30]Schuster J, He G, Mandlmeier B, et al. *Angew. Chem. Int. Ed.*, **2012**,**51**:3591-3595

[31]He G, Ji X L, Nazar L. *Energ. Environ. Sci.*, **2011**,**4**:2878-2883

[32]Tao X Y, Chen X Y, Xia Y, et al. *J. Mater. Chem. A*, **2013**, **1**:3295-3301

[33]Zheng G Y, Yang Y, Cha J J, et al. *Nano Lett.*, **2011**,**11**: 4462-4467

[34]Guo J C, Xu Y H, Wang C S. *Nano Lett.*, **2011**,**11**:4288-4294

[35]Ji L W, Rao M M, Aloni S, et al. *Energ. Environ. Sci.*, **2011**,**4**:5053-5059

[36]Elazari R, Salitra G, Garsuch A, et al. *Adv. Mater.*, **2011**, **23**:5641-5644

[37]Li W, Zhang F, Dou Y Q, et al. *Adv. Energy Mater.*, **2011**, **1**:382-386